Journal of Applied Geophysics 159 (2018) 690–696

Contents lists available at ScienceDirect

Journal of Applied Geophysics

journal homepage: www.elsevier.com/locate/jappgeo

Moveout approximation for a P-SV wave in a moderately anisotropic homogeneous DTI layer

Véronique Farra [a], Ivan Pšenčík [b,*]

[a] Institut de Physique du Globe de Paris, Sorbonne Paris Cité, UMR 7154 CNRS, Paris, France
[b] Institute of Geophysics, Acad. Sci. of CR, Boční II, 141 31 Praha 4, Czech Republic

ARTICLE INFO

Article history:
Received 10 August 2018
Received in revised form 21 September 2018
Accepted 9 October 2018
Available online xxxx

ABSTRACT

We derive and test the moveout formula for converted P-SV (or SV-P) waves in a homogeneous, weakly or moderately anisotropic, transversely isotropic layer with axis of symmetry perpendicular to a dipping reflector underlying it. Instead of commonly used Taylor series expansion of the squared traveltime with respect to the offset, we use weak-anisotropy approximation of the exact traveltime formula. We replace the exact traveltime along the actual ray of a converted wave by its first-order weak-anisotropy approximation along a ray in a nearby reference isotropic medium. The traveltime formula is derived in the plane defined by the source-receiver line and the normal to the reflector. The source and the receiver may be situated arbitrarily in the model, the flat reflector may have an arbitrary 3D orientation. The accuracy of the proposed moveout formula is tested on models with varying strength of anisotropy for a varying dip of the reflector. In isotropic media, the formula yields highly accurate results with relative traveltime errors not exceeding 0.5%. In anisotropic media of P- and SV-wave anisotropy of about 25% and 12%, respectively, relative traveltime errors do not exceed 2%.

1. Introduction

Reflection moveout approximations are a broadly used tool for the velocity-model building. They provide relation between observed traveltimes and parameters of a medium, which is generally considered to be anisotropic. Reflection moveout is most often used in the connection with unconverted waves. Applications to converted (mostly PS) waves are also numerous. They are mostly related to transversely isotropic media with vertical axis of symmetry (VTI media), see for example, Seriff and Sriram (1991), Tsvankin and Thomsen (1994), Granli et al. (1999), Thomsen (1999), Tsvankin and Grechka (2000), Li and Yuan (2003), Hao and Stovas (2016). Detailed reviews of moveout of converted waves can be found in monographs Tsvankin (2001), Tsvankin and Grechka (2011).

We seek an approximate formula for the square of the reflection time T^2 as a function of the offset x (source-receiver distance) assuming that anisotropy of the medium is weak. The formula obtained in this way represents the first-order approximation of exact formula in terms of the weak-anisotropy (WA) parameters, which characterize deviations of anisotropy from isotropy. In all previous studies, see for example, Farra et al. (2016), such approximations provided sufficiently accurate results not only for weakly, but also for moderately anisotropic media with anisotropy strength varying between 20 and 30%. Their comparison with commonly used approximations in situations, in which both approaches are applicable (commonly used formulae are usually applicable to only limited types of models) yields results of comparable or even better accuracy.

In this paper, we generalize the formula of Farra and Pšenčík (2017) for the moveout of converted waves in a homogeneous, moderately anisotropic, transversely isotropic (TI) layer with a vertical axis of symmetry (VTI) underlaid by a horizontal reflector to the case of a dip-constrained TI (DTI) medium, whose symmetry axis is perpendicular to the dipping reflector. We thus deal with a 3D experiment: an arbitrary oriented surface profile over an arbitrarily oriented plane reflector. Although such a structure represents a simplification of reality, it can find its counterparts in dipping shale formations in overthrust areas (Tsvankin, 2001). More details about DTI media can be found, for example, in Alkhalifah and Sava (2010) or Golikov et al. (2012). The formula derived in this paper can be applied along an arbitrarily chosen source-receiver profile over an arbitrarily oriented plane reflector. The formula depends on WA parameters specifying the DTI medium and on the apparent dip angle φ_{AD} of the reflector. The apparent dip angle is the angle between the profile and the intersection of the reflector with the plane containing the profile and the normal to the reflector.

The paper has the following structure. In Sec. 2, we describe the configuration of the reflection experiment and introduce the notation. In Sec. 3, we present traveltime expressions along the P- and SV-wave ray legs, and introduce approximations necessary for their evaluation. With all the necessary formulae introduced, it is possible to present

* Corresponding author.
E-mail address: ip@ig.cas.cz (I. Pšenčík).

https://doi.org/10.1016/j.jappgeo.2018.10.011
0926-9851/

expressions for the P-SV-wave moveout in Sec. 4. The following Sec. 5 offers tests of accuracy of the derived formulae on an isotropic and three anisotropic models of a homogeneous layer over a dipping reflector. The paper ends by conclusions listed in Sec. 6. In Appendix A, we offer two possibilities how to determine the conversion point in a reference isotropic medium. Appendix B contains definitions of weak-anisotropy (WA) parameters used in this study.

2. Configuration of the experiment

Let us consider a weakly or moderately anisotropic homogeneous transversely isotropic (TI) layer underlaid by an arbitrarily oriented dipping plane reflector. The axis of symmetry of the TI medium is assumed to be perpendicular to the reflector. We are thus dealing with the dip-constrained TI (DTI) medium. Let us concentrate on the plane containing the source-receiver profile and the normal to the reflector. The configuration of the experiment in this plane is shown in Fig. 1. The reflector makes an apparent dip angle φ_{AD}, positive clockwise, with the source-receiver profile. The apparent dip of the reflector depends on the actual dip of the reflector and on the orientation of the source-receiver profile. For the determination of the apparent dip angle φ_{AD} from these factors, see Farra and Pšenčík (2013b). The distance $\bar{SR}$ between the source S and the receiver R is the offset x. The point O is the common midpoint and the point C is a perpendicular projection on the source-receiver profile of the conversion point C', situated on the reflector. The distance $\bar{SC}$ is the offset x_C of the conversion point. Perpendicular projections of the source S, the receiver R and the common midpoint O on the reflector are denoted by S', R' and O', respectively. The distances $\bar{SS'}$, $\bar{RR'}$ and $\bar{OO'}$ are denoted H_S, H_R and H, respectively.

Although the anisotropy of the considered medium belongs to simpler ones, to determine the ray path of a converted P-SV wave between the points S and R is not an easy task. In principle, the solution of two-point ray tracing problem is required here. To avoid it, we consider a nearby P-S-wave ray path in a reference isotropic medium with P- and S-wave velocities α and β, respectively, instead of the exact P-SV-wave ray path. The actual ray is thus replaced by the ray whose deviation from the actual ray is assumed to be of the first order. This results in the second-order traveltime error (Fermat's principle). The offset x_C of the conversion point is thus sought in the reference isotropic medium. The conversion-point dispersal (Tsvankin, 2001) is implicitly incorporated in the approach. As shown in Fig. 1, the down-going P-wave reference ray leg makes the angle θ_P and the up-going S-wave reference ray leg makes the angle θ_S with the normal to the reflector at the conversion point C'. To find the conversion point C' in the reference isotropic medium is feasible although even this is not an easy task. In Appendix A, we show how to determine the conversion point in the reference isotropic medium either by solving numerically a quartic equation or by using an approximate formula representing its solution. It is shown in Appendix A that the position of the conversion point depends on the ratio r of S- and P-wave velocities in the reference isotropic medium, $r = \beta/\alpha$, and on the apparent dip angle of the reflector φ_{AD}. The ratio r can be determined as a constant from available estimates of α and β. For an efficient application of Fermat's principle, it is, however, desirable to choose r as close as possible to the ratio of SV- and P-wave velocities of the studied actual medium.

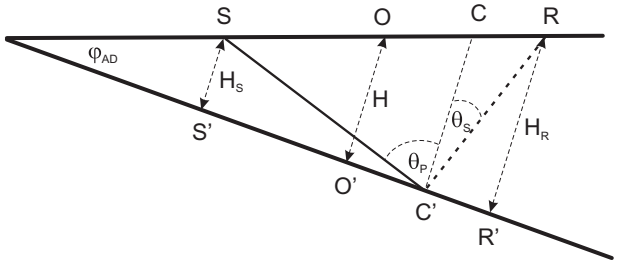

Fig. 1. Schematic plot of a ray of a converted P-S wave in the reference isotropic medium, reflected from the dipping reflector, with φ_{AD} representing the apparent dip angle. H_S, H_R and H are orthogonal distances of the source S, the receiver R and common midpoint O from the reflector, respectively. S', R' and O' are projections of S, R and O, respectively to the reflector. The point C' is the conversion point and C is its projection on the source-receiver profile. θ_P and θ_S are angles of incidence and reflection, respectively.

3. Traveltime formula

Let us denote by N_P and N_S unit vectors (ray vectors) tangent to the down-going P-wave and up-going S-wave reference ray legs, respectively. We can then write expressions for the squares of traveltime along the P- and S-wave ray legs in the following way, see Fig. 1:

$$T_P^2(x) = \frac{x_C^2\,\cos^2\varphi_{AD} + H_S^2}{v_P^2\left(\mathbf{N}^P\right)}, \qquad T_{SV}^2(x) = \frac{(x-x_C)^2\,\cos^2\varphi_{AD} + H_R^2}{v_{SV}^2\left(\mathbf{N}^S\right)} \quad . \tag{1}$$

In Eq. (1), $v_P(\mathbf{N}^P)$ and $v_{SV}(\mathbf{N}^S)$ denote P- and SV-wave ray velocities in the DTI medium.

Let us introduce the one-way zero-offset traveltimes T_{HS} and T_{HR} at the source and the receiver in the reference isotropic medium:

$$T_{HS} = \frac{H_S}{\alpha} = \frac{H - \frac{1}{2}x\,\sin\varphi_{AD}}{\alpha}, \qquad T_{HR} = \frac{H_R}{\beta} = \frac{H + \frac{1}{2}x\,\sin\varphi_{AD}}{\beta} \quad . \tag{2}$$

Let us also introduce normalized projections to the reflector of the distance x_C of the conversion point C from the source S ($\bar{S'C'}$) and of the distance $x - x_C$ ($\bar{C'R'}$) of the receiver R from the conversion point C in the following way:

$$\check{x}_C = \frac{x_C\,\cos\varphi_{AD}}{H_S}, \qquad \hat{x} - \hat{x}_C = \frac{(x-x_C)\,\cos\varphi_{AD}}{H_R} \quad . \tag{3}$$

With the notation introduced in Eqs. (2) and (3), Eq. (1) receives the form:

$$T_P^2(x) = T_{HS}^2\alpha^2\,\frac{1+\check{x}_C^2}{v_P^2\left(\mathbf{N}^P\right)}, \qquad T_{SV}^2(x) = T_{HR}^2\beta^2\,\frac{1+(\hat{x}-\hat{x}_C)^2}{v_{SV}^2\left(\mathbf{N}^S\right)} \quad . \tag{4}$$

For the evaluation of traveltime formulae in Eq. (4), it remains to find the expressions for P- and SV-wave ray velocities. Instead of complicated exact expressions, we use their first-order approximations. We can use expressions of Farra and Pšenčík (2017) if, instead of the general Cartesian coordinate system, we use a local Cartesian coordinate system related to the reflector. Its x_1-axis is situated along the intersection of the reflector with the plane containing the source-receiver profile and the normal to the reflector. The x_3-axis is perpendicular to the reflector, positive downwards. Unit vectors N^P and N^S are thus situated in the plane (x_1,x_3) of the local coordinate system. Their non-zero components are

$$N_1^P = \frac{\check{x}_C}{\sqrt{1+\check{x}_C^2}}, \qquad N_3^P = \frac{1}{\sqrt{1+\check{x}_C^2}} \tag{5}$$

for P wave and

$$N_1^S = \frac{\hat{x}-\hat{x}_C}{\sqrt{1+(\hat{x}-\hat{x}_C)^2}}, \qquad N_3^S = -\frac{1}{\sqrt{1+(\hat{x}-\hat{x}_C)^2}} \tag{6}$$

for S wave.

We can now use expressions (12) and (13) of Farra and Pšenčík (2017) for P- and SV-wave ray velocities of a converted wave reflected

at a horizontal reflector, and use them in the local Cartesian coordinate system related to the reflector. The approximate expression for the P-wave ray velocity has the form:

$$\widetilde{v_P^2}\left(\mathbf{N}^P\right) \sim \widetilde{c_P^2}\left(\mathbf{N}^P\right) \sim \alpha^2\left\{1+2\left[\epsilon_x\left(N_1^P\right)^4+\delta_y\left(N_1^P\right)^2\left(N_3^P\right)^2+\epsilon_z\left(N_3^P\right)^4\right]\right\}. \tag{7}$$

The approximate expression for the SV-wave ray velocity reads:

$$\widetilde{v_{SV}^2}\left(\mathbf{N}^S\right) \sim \widetilde{c_{SV}^2}\left(\mathbf{N}^S\right) \sim \beta^2\left[1+2\gamma_y+2r^{-2}(\epsilon_x+\epsilon_z-\delta_y)\left(N_1^S\right)^2\left(N_3^S\right)^2\right] \quad . \tag{8}$$

Tildes over symbols indicate that the corresponding quantities are of the first order in the weak-anisotropy approximation. Symbols c_P and c_{SV} denote P- and SV-wave phase velocities. Symbols ϵ_x, ϵ_z, δ_y and γ_y are WA parameters related to the reflector coordinate system. They are defined in Appendix B.

4. P-SV-wave moveout

By inserting expressions (5) and (6) to equations for the ray velocities (7) and (8), and by inserting the resulting equations to the traveltime formulae (4), we obtain:

$$T_P^2(x) = T_{HS}^2\frac{\left(1+\check{x}_C^2\right)^3}{P_P(\check{x}_C)}, \quad T_{SV}^2(x) = T_{HR}^2\frac{\left[1+(\hat{x}-\hat{x}_C)^2\right]^3}{P_{SV}(\hat{x}-\hat{x}_C)} \quad . \tag{9}$$

The normalized offsets $\check{x}_C$, $\hat{x}_C$ and $\hat{x}$ are related to the offsets x_C and x through the expressions given in Eq. (3). Symbols $P_P(x)$ and $P_{SV}(x)$ denote polynomials, which, due to the use of the local coordinate system related to the reflector, have identical form with the polynomials derived by Farra and Pšenčík (2017). They read:

$$P_P(x) = \left(1+x^2\right)^2+2\epsilon_x x^4+2\delta_y x^2+2\epsilon_z \tag{10}$$

and

$$P_{SV}(x) = \left(1+x^2\right)^2\left(1+2\gamma_y\right)+2r^{-2}(\epsilon_x+\epsilon_z-\delta_y)x^2 \quad . \tag{11}$$

With all the above expressions, we are now able to write the final expression for the square of the total traveltime $T(x) = T_P(x) + T_{SV}(x)$:

$$T^2(x) = \left[T_{HS}\frac{\left(1+\check{x}_C^2\right)^{3/2}}{P_P^{1/2}(\check{x}_C)}+T_{HR}\frac{\left[1+(\hat{x}-\hat{x}_C)^2\right]^{3/2}}{P_{SV}^{1/2}(\hat{x}-\hat{x}_C)}\right]^2 \quad . \tag{12}$$

To evaluate Eq. (12), we have to take into account Eqs. (2) and (3) for T_{HS}, T_{HR}, $\check{x}_C$ and $\hat{x}-\hat{x}_C$, and also Eqs. (10) and (11) for polynomials $P_P(x)$ and $P_{SV}(x)$. Because the offset of the conversion point x_C depends on the ratio of S- and P-wave velocities in the reference isotropic medium and on the apparent dip angle φ_{AD} of the reflector, the formula (12) itself depends on the choice of the parameters of the reference medium and φ_{AD} too.

In the isotropic case, which we also test in the following section, Eq. (12) reduces to the form:

$$T^2(x) = \left[T_{HS}\left(1+\check{x}_C^2\right)^{1/2}+T_{HR}\left[1+(\hat{x}-\hat{x}_C)^2\right]^{1/2}\right]^2 \quad . \tag{13}$$

Definitions of quantities T_{HS}, T_{HR}, $\check{x}_C$ and $\hat{x}-\hat{x}_C$ can be again found in Eqs. (2) and (3). For the exact value of the conversion offset x_C, Eq. (13) yields the exact traveltime.

Transformation of Eqs. (12) or (13) into the form of the commonly used Taylor series expansion of the squared traveltime with respect to the offset would lead to an expansion with non-zero odd terms. It is because the considered DTI configuration is asymmetric with respect to the zero offset, see Tsvankin and Grechka (2011). It is easy to derive the coefficients of such an expansion from Eqs. (12) or (13). Here we present only the first coefficient corresponding to the zero-offset traveltime for the DTI configuration. It reads:

$$T^2(0) = \left[T_{HS}(1+2\epsilon_z)^{-1/2}+T_{HR}\left(1+2\gamma_y\right)^{-1/2}\right]^2 \quad . \tag{14}$$

Eq. (14) is exact. Expressed in terms of elastic parameters in the Voigt notation, it yields $T(0) = H_S A_{33}^{-1/2} + H_R A_{55}^{-1/2}$. In the isotropic case, Eq. (14) reduces to the obvious $T(0) = H_S\alpha^{-1} + H_R\beta^{-1}$.

5. Tests of accuracy

We test accuracy of Eqs. (12) and (13) for converted P-SV waves in four models with reflectors of varying dip. The first model is isotropic, the remaining three models are DTI models with varying strength of P- and SV-wave anisotropy. The models have been used by Farra and Pšenčík (2017) for the study of accuracy of approximate moveout formulae for waves converted at a horizontal reflector. The P- and S-wave velocities of the isotropic model are $\alpha = 2.5$ km/s and $\beta = 1$ km/s, respectively. The parameters of anisotropic models are given in Table 1. The P- and S-wave reference velocities α and β, respectively, are chosen as P- and SV-wave velocities along the axes of symmetry of the considered models. This choice allows a comparison with results of previous studies. It leads to $\epsilon_z = \gamma_y = 0$, and thus to the reduction of the number of involved WA parameters from four to two, ϵ_x and δ_y. The three anisotropic models are the limestone model, whose P- and SV-wave anisotropies are ~ 8% and ~ 5%, respectively, and the Mesaverde mudshale and the hard shale models with P-wave anisotropies ~ 6% and ~ 25%, respectively, and SV-wave anisotropy of ~ 12%. The anisotropy strength is defined as $2(c_{max} - c_{min})/(c_{max} + c_{min}) \times 100\%$, where c denotes corresponding phase velocity. Let us add that the first two models have $\epsilon_x - \delta_y$ negative while the third has $\epsilon_x - \delta_y$ positive.

In the following figures, we present plots of relative traveltime errors $(T - T_{ex})/T_{ex} \times 100\%$. Here T is the traveltime calculated from Eqs. (12) or (13) and T_{ex} is the traveltime calculated using the package ANRAY (Gajewski and Pšenčík, 1990), which we take as an exact reference.

Each of the following figures contains two plots with relative traveltime errors. The a) plots contain curves for the conversion point x_C obtained by numerical solution of the quartic equation (A-4), and the b) plots contain curves obtained from the approximate formula (A-7) with coefficients C_0 to C_3 determined from Eqs. (A-8) and (A-10). The curves of different colours correspond to different reflector dips. Black curves correspond to the horizontal reflector and are identical with curves shown by Farra and Pšenčík (2017) for the corresponding models. Red, blue, green and light blue curves correspond to the apparent dip angles $\varphi_{AD} = 10^\circ, 20^\circ, -10^\circ$, and -20°, respectively.

First we show results obtained from Eq. (13) for the isotropic layer. Numerical solution of the quartic equation (A-4) to determine the offset x_C of the conversion point leads to exact results. It is because we use the exactly determined conversion point and thus actual ray trajectory.

Table 1
Parameters of the anisotropic models used. α and β - P- and S-wave reference velocities, ϵ_x, δ_y, ϵ_z and γ_y - WA parameters.

Model	α (km/s)	β (km/s)	ϵ_x	δ_y	ϵ_z	γ_y
Limestone	3.0	1.707	0.076	0.133	0.	0.
Mesaverde mudshale	4.53	2.703	0.034	0.184	0.	0.
Hard shale	3.0	1.914	0.252	0.034	0.	0.

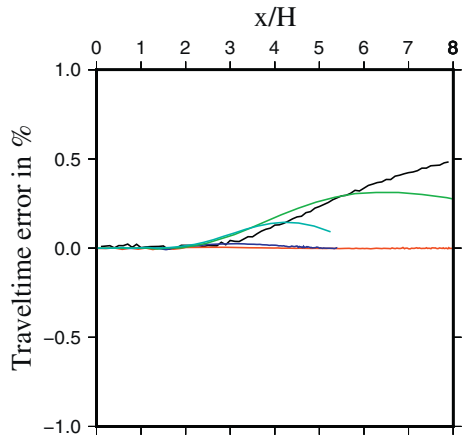

Fig. 2. P-SV-wave moveout in the isotropic layer ($\alpha = 2.5$ km/s, $\beta = 1.$ km/s) with the reflector of varying dip φ_{AD}, $\varphi_{AD} = 0^{\circ}$ - black, $\varphi_{AD} = 10^{\circ}$ - red, $\varphi_{AD} = 20^{\circ}$ - blue, $\varphi_{AD} = -10^{\circ}$ - green, $\varphi_{AD} = -20^{\circ}$ - light blue. Variation with the normalized offset x/H of the relative traveltime error with the conversion point determined from approximate Eq. (A-7) with C_i defined in (A-8) and (A-10).

Determination of x_C from the approximate formula (A-7) with coefficients C_0 to C_3 given in (A-8) and (A-10) results in non-zero traveltime errors shown in Fig. 2. The traveltime errors of the reflections from the reflector with a positive dip remain negligible, but errors for the negative dips, and especially for the zero dip reach nearly 0.5% for the normalized offset x/H~8. The reason for these larger errors are larger deviations of x_C determined from the approximate Eq. (A-7) from the exact values of x_C determined from Eq. (A-4); compare the dashed and solid curves in Fig. 6 in Appendix A. In Fig. 2, we can see that due to the stronger dip of the reflector, blue ($\varphi_{AD} = 20^{\circ}$) and light blue ($\varphi_{AD} = -20^{\circ}$) curves terminate at $x_{max}/H < 8$.

In Fig. 3, which shows results for the anisotropic limestone layer, even the use of numerical solution of the quartic equation (A-4) leads to observable errors, see Fig. 3a. It is because traveltime is calculated along reference and not actual rays. Nevertheless, the errors do not exceed 0.2%. They are larger for positive dips of the reflector. This is caused by the application of the less accurate approximation of SV-wave ray velocity along longer S-wave ray path, compare Figs. 1 and 3 of Farra and Pšenčík (2013a). The effect is even more pronounced when the approximate Eq. (A-7) for the determination of x_C is used, see Fig. 3b. In this case the maximum errors may reach 0.5%.

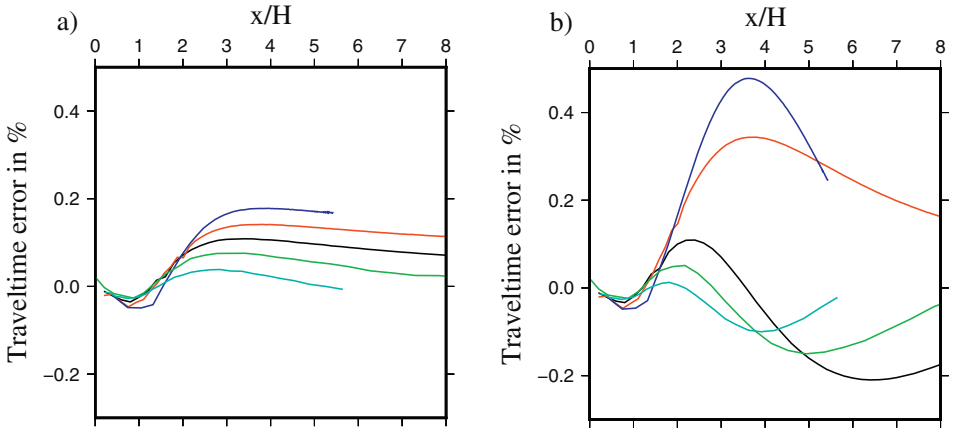

Fig. 3. P-SV-wave moveout in the limestone model, P-wave anisotropy ~ 8%, SV-wave anisotropy ~ 5%, with the reflector of varying dip φ_{AD}, $\varphi_{AD} = 0^{\circ}$ - black, $\varphi_{AD} = 10^{\circ}$ - red, $\varphi_{AD} = 20^{\circ}$ - blue, $\varphi_{AD} = -10^{\circ}$ - green, $\varphi_{AD} = -20^{\circ}$ - light blue. Variation with the normalized offset x/H of the relative traveltime error with the conversion point determined a) by the numerical solution of Eq. (A-4); b) from approximate Eq. (A-7) with C_i defined in (A-8) and (A-10).

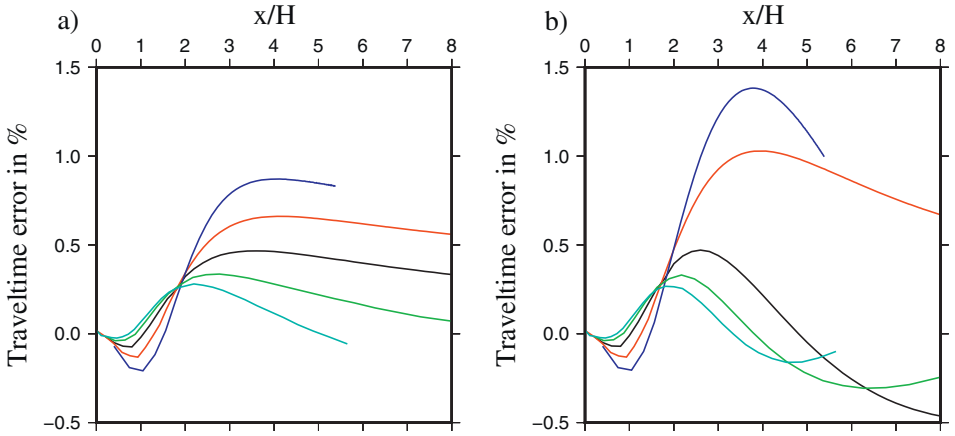

Fig. 4. P-SV-wave moveout in the Mesaverde mudshale model, P-wave anisotropy ~ 6%, SV-wave anisotropy ~ 12%, with the reflector of varying dip φ_{AD}, $\varphi_{AD} = 0^{\circ}$ - black, $\varphi_{AD} = 10^{\circ}$ - red, $\varphi_{AD} = 20^{\circ}$ - blue, $\varphi_{AD} = -10^{\circ}$ - green, $\varphi_{AD} = -20^{\circ}$ - light blue. Variation with the normalized offset x/H of the relative traveltime error with the conversion point determined a) by the numerical solution of Eq. (A-4); b) from approximate Eq. (A-7) with C_i defined in (A-8) and (A-10).

Similar features as in Fig. 3, can be observed in Fig. 4. Traveltime errors are, however, larger because SV-wave anisotropy is slightly stronger in the Mesaverde mudshale model. This is in accord with Figs. 3 and 4 of Farra and Pšenčík (2013a). Traveltime errors obtained with x_C determined from Eq. (A-4) are, however, still <1%, see Fig. 4a. Determination of x_C from the approximate formula (A-7) leads to slightly higher errors, which are, however, still <1.5%, see Fig. 4b. Larger errors are observed for reflectors with positive dips. For horizontal reflectors or for reflectors with negative dips, the errors are <0.5% no matter if they are determined by the numerical solution of Eq. (A-4) or from approximate Eq. (A-7). The reason for larger errors for reflectors with positive dips is the same as in Fig. 3.

Results shown for hardshale layer shown in Fig. 5 have slightly different character than the results in Figs. 3 and 4. First, P-wave anisotropy of the hardshale model is considerably stronger than in the other models. As a consequence, maximum relative traveltime errors approach 2%. Second, and probably more importantly, hardshale model has the parameter ϵ_x much stronger than in other models, see Table 1. Third, in contrast to the previous models, the term $\epsilon_x - \delta_y$ is positive for the hardshale model. As Farra and Pšenčík (2013a) point out, variation of the SV-wave phase velocity with offset has a different character than in limestone and Mesaverde mudshale models, compare Fig. 5a with Figs. 3a and 4a of Farra and Pšenčík (2013a). As a result, in contrast to other models, traveltime errors in the hardshale model do not depend so strongly on the dip of the reflector as they do in other models.

6. Conclusions

In the previous sections we generalized the formula of Farra and Pšenčík (2017) for the moveout of converted waves in a homogeneous, moderately anisotropic, VTI layer underlaid by a horizontal reflector to the case of a dip-constrained medium with an arbitrary oriented plane reflector. The formula is applicable along an arbitrarily chosen source-receiver surface profile, which makes the experiment 3D. As Farra and Pšenčík (2017), we made two important approximations. Instead of actual rays of converted waves we considered reference rays in a nearby reference isotropic medium. Along these rays, we used first-order approximations of P- and SV-wave ray velocities.

As in the paper of Farra and Pšenčík (2017), an important part of the determination of the moveout is the determination of the conversion point on the reflector. This can be done by solving numerically a quartic equation or by using its approximate solution. Special attention is paid to the generalization of the approximate solution for the case of a dipping reflector, see Appendix A. Due to the existence of the reflector dip, the normalized offset has a limited extent. The larger the dip, the shorter the maximum offset. For the horizontal reflector (zero dip), the presented formula reduces to the moveout formula of Farra and Pšenčík (2017).

If the conversion point is determined by the numerical solution of the quartic equation (A-4), the presented formula for the isotropic case yields exact results. In anisotropic media, the maximum relative traveltime errors do not exceed 2% for P- and SV-wave anisotropy of approximately 25% and 12%, respectively.

The derived formula depends a) on 4 WA parameters, ϵ_x, ϵ_z, δ_y and γ_y, specifying the TI medium, b) on the apparent dip angle φ_{AD} made by the source-receiver profile with the intersection of the reflector with the plane containing the profile and the normal to the reflector, and c) on the ratio r of the reference velocities. The apparent dip angle relates to the quantities specifying the orientation of the profile and the reflector, see Farra and Pšenčík (2013b).

We did not try to rewrite Eqs. (12) and (13) in the commonly used form of a Taylor series expansion of squared traveltime T^2 with respect to the offset x because the studied moveout for the DTI configuration is asymmetric with respect to the zero offset (Tsvankin and Grechka, 2011). As a consequence, the Taylor series expansion of T^2 contains not only even but also odd terms with x. This, as Tsvankin and Grechka (2011) point out, makes the notion of the NMO velocity and of the quartic term of the traveltime expansion meaningless. The symmetry of the moveout is achieved for the zero apparent dip angle.

The presented formula is applicable to both P-SV and SV-P waves. It is because one can exchange the positions of the source and the receiver keeping the wave modes along the ray legs unchanged.

More realistic than the DTI medium considered in this paper would probably be a dip-constrained orthorhombic medium. Derivation of approximate moveout formula for P-S or S-P waves in such a medium will be more involved. The separation of S waves into SV and SH waves, used in the studied DTI medium, is impossible in orthorhombic media. Approximate traveltime formulae for separate S waves are more complicated. One option would be to consider traveltimes of a common S wave (Farra and Pšenčík, 2010) instead of traveltimes of two separate S waves.

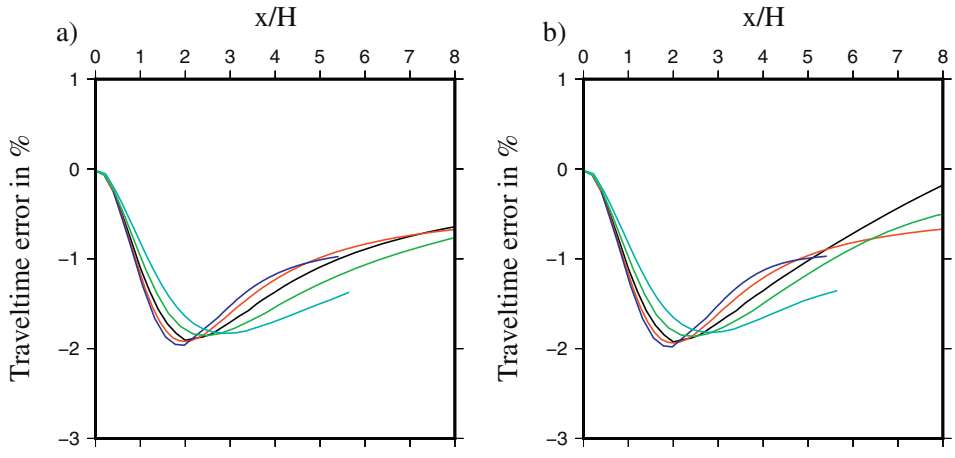

Fig. 5. P-SV-wave moveout in the hardshale model, P-wave anisotropy ~ 25%, SV-wave anisotropy ~ 12%, with the reflector of varying dip φ_{AD}, $\varphi_{AD} = 0^\circ$ - black, $\varphi_{AD} = 10^\circ$ - red, $\varphi_{AD} = 20^\circ$ - blue, $\varphi_{AD} = -10^\circ$ - green, $\varphi_{AD} = -20^\circ$ - light blue. Variation with the normalized offset x/H of the relative traveltime error with the conversion point determined a) by the numerical solution of Eq. (A-4); b) from approximate Eq. (A-7) with C_i defined in (A-8) and (A-10).

Acknowledgement

We thank Alexey Stovas and an anonymous referee for constructive comments. A substantial part of this work was done during IP's stays at the IPG Paris. We are grateful to the Research Project 16-05237S of the Grant Agency of the Czech Republic and the project "Seismic waves in complex 3-D structures" (SW3D) for support.

Appendix A. Determination of the conversion point in the reference isotropic medium

Let us consider a homogeneous *isotropic* layer underlaid by a dipping reflector with the apparent dip angle φ_{AD}, see Fig. 1. For the determination of φ_{AD} from the actual dip and azimuth of the source-receiver profile see Farra and Pšenčík (2013b). In the medium above the reflector, we consider the source S and the receiver R. The distance between these two points is the offset x. Let us consider a ray of a converted P-S wave between the points S and R, with the conversion point C' at the reflector, see Fig. 1. Its perpendicular projection on the surface is the conversion point C, situated at the offset x_C. Its position, of course, differs from the position of the midpoint O, the point in the middle of the offset x. We denote by α and β P- and S-wave velocities, respectively, and by $r = \beta/\alpha$ their ratio. The angles of incidence and reflection of a ray of the converted P-S wave are denoted by θ_P and θ_S, respectively. The orthogonal distances of the source S and the receiver R from the reflector are H_S and H_R, respectively. The distances H_S and H_R can be expressed in terms of the orthogonal distance H of the common midpoint O from the reflector, and the apparent dip angle φ_{AD} as

$$H_S = H - \frac{x}{2}\,\sin\varphi_{AD}, \quad H_R = H + \frac{x}{2}\,\sin\varphi_{AD} \quad , \qquad (A-1)$$

see Eq. (2) of Farra and Pšenčík (2013b).

Since the source S and the receiver R are situated above the reflector, one must require $H_S \geq 0$ and $H_R \geq 0$. This implies that in the case of a dipping reflector, the offset x cannot be infinite as in the case of the horizontal reflector. For a dipping reflector, the offset x may reach, at maximum, its limiting value x_{max}:

$$x_{max} = \frac{2H}{|\,\sin\varphi_{AD}\,|} \quad . \qquad (A-2)$$

For the positive apparent dip angle φ_{AD} and for the offset x_{max}, Eq. (A-1) yields $H_S = 0$ and $H_R = 2H$. For the negative apparent dip angle φ_{AD} and for the offset x_{max}, Eq. (A-1) yields $H_S = 2H$ and $H_R = 0$. This is an obvious consequence of the relation $2H = H_S + H_R$, which follows from Eq. (A-1).

Elementary trigonometry considerations based on the sketch in Fig. 1 yield the following expressions for $\sin\theta_P$ and $\sin\theta_S$:

$$\sin\theta_P = \frac{x_C\,\cos\varphi_{AD}}{\sqrt{x_C^2\,\cos^2\varphi_{AD} + H_S^2}}, \qquad \sin\theta_S = \frac{(x - x_C)\,\cos\varphi_{AD}}{\sqrt{(x-x_C)^2\,\cos^2\varphi_{AD} + H_R^2}} \quad . \qquad (A-3)$$

Combination of Eq. (A-3) with the Snell law, $\sin\theta_P/\alpha = \sin\theta_S/\beta$, leads, after some manipulation, to the equation

$$x_C^4 - 2x_C^3 x + x_C^2\left(x^2 + \frac{H_R^2 r^2 - H_S^2}{Q(r,\varphi_{AD})}\right) + 2x_C\frac{H_S^2 x}{Q(r,\varphi_{AD})} - \frac{H_S^2 x^2}{Q(r,\varphi_{AD})} = 0 \quad , \qquad (A-4)$$

where

$$Q(r,\varphi_{AD}) = (r^2 - 1)\,\cos^2\varphi_{AD} \quad . \qquad (A-5)$$

Eq. (A-4) is a quartic polynomial equation for the offset of the conversion point x_C. For the horizontal reflector, $\varphi_{AD} = 0^\circ$, Eq. (A-4) reduces to Eq. (4) of Farra and Pšenčík (2017). It is of interest to note that for the case of an unconverted reflection from a dipping reflector, it is for the ratio of velocities of generated and incident waves $r = 1$, Eq. (A-4) yields

$$x_C = \frac{x}{2}\frac{H_S}{H} \quad , \qquad (A-6)$$

which reduces to the expected $x_C = x/2$ for the horizontal reflector. Eq. (A-4) can be solved numerically or approximately.

Numerical solution of Eq. (A-4) leads to four roots, of which only one lies in the interval $(0, x)$, and it is the sought root.

For an approximate solution, one can use a generalization by Thomsen (1999) of the approximate formula for the determination of the conversion point proposed by Tessmer and Behle (1988) for an isotropic layer over a horizontal reflector. Thomsen (1999) sought the approximate solution of his quartic equation in the form of a modified Taylor series expansion. In our case the modified Taylor series expansion has the form:

$$x_C \sim x\left[C_0 + \frac{C_1(x/H) + C_2(x/H)^2}{1 + C_3(x/H)^2}\right] \quad . \qquad (A-7)$$

The coefficients in Eq. (A-7) are sought so that (A-7) satisfies asymptotically Eq. (A-4) for minimum and maximum offsets. The coefficients C_0, C_1 and C_2 are obtained by inserting Eq. (A-7) to the quartic equation (A-4) and taking limit $x \to 0$. We get

$$C_0 = \frac{1}{1+r}, \quad C_1 = -\frac{r\,\sin\varphi_{AD}}{(1+r)^2} \quad , \quad C_2 = \frac{r}{2}\frac{1-r}{(1+r)^3}\,\cos 2\varphi_{AD} \quad . \qquad (A-8)$$

The coefficient C_3 is obtained from the limit $x \to x_{max}$.

In the case of a horizontal reflector, $\varphi_{AD} = 0^\circ$, for $x \to \infty$, we get from the quartic Eq. (A-4) $x_C/x \to 1$. Inserting this to Eq. (A-7), we obtain

$$C_3 = \frac{1}{2}\frac{1-r}{(1+r)^2} \quad , \qquad (A-9)$$

see Thomsen (1999).

In the case of a dipping reflector, the offset x can reach, at maximum, the value x_{max}. The coefficient C_3 should be chosen so that Eq. (A-7) yields the limiting value x_{Clim} of x_C for $x = x_{max}$. Inserting $x = x_{max}$ to Eq. (A-7), we obtain:

$$C_3 = \frac{1}{2}\frac{C_1\,|\,\sin\varphi_{AD}\,| + 2C_2}{\bar{x}_{Clim} - C_0} - \frac{1}{4}\,\sin^2\varphi_{AD} \quad , \qquad (A-10)$$

where $\bar{x}_{Clim} = x_{Clim}/x_{max}$. For a horizontal reflector, for which $\bar{x}_{Clim} = 1$, Eq. (A-10) reduces to Eq. (A-9), i.e., to the result obtained earlier by Thomsen (1999).

The inspection of Eq. (A-7) at the offset $x = 0$ shows that the value of the ratio x_C/x is controlled by the coefficient C_0 and the slope of x_C/x as a function of x/H is controlled by C_1. For $\varphi_{AD} < 0^\circ$, the slope is positive, the projection C of the conversion point to the source-receiver profile tends to approach the receiver R. For $\varphi_{AD} = 0^\circ$, the slope is zero. For $\varphi_{AD} > 0^\circ$, the slope is negative, the point C tends to approach the source S.

Let us now seek the limiting value x_{Clim}, situated in the interval $0 \leq x_{Clim} \leq x_{max}$, i.e., $0 \leq \bar{x}_{Clim} \leq 1$, separately for the case of a dipping reflector with the negative ($\varphi_{AD} < 0^\circ$) and positive ($\varphi_{AD} > 0^\circ$) apparent dip.

For $\varphi_{AD} < 0^\circ$ and $x = x_{max}$, we get $H_R = 0$, see the discussion after Eq. (A-2). It is easy to prove that

$$\bar{x}_{Clim} = 1 \qquad (A-11)$$

is an acceptable solution of Eq. (A-4). In this case the receiver R is situated at the intersection of the reflector with the profile ($H_R = 0$). The

P-wave ray leg is parallel to the profile and the conversion point coincides with R.

For $\varphi_{AD} > 0^\circ$ and $x = x_{max}$, the situation is more complicated. In this case, we get $H_S = 0$ and acceptable solutions of Eq. (A-4) are

$$\bar{x}_{Clim} = 0 \quad \text{and} \quad \bar{x}_{Clim} = \left(1 - \tan\theta_S^* \tan\varphi_{AD}\right) . \qquad (A-12)$$

Here θ_S^* is the critical angle, $\sin\theta_S^* = r$. In this case, the source S is situated at the intersection of the reflector with the profile ($H_S = 0$). The second equation in (A-12) yields $\bar{x}_{Clim}$ in the interval $0 \le \bar{x}_{Clim} < 1$ if $\tan\theta_S^* \tan\varphi_{AD} \le 1$. In this case, the P-wave ray leg is tangent to the reflector, and S-wave ray leg leaves the reflector at the conversion point under the angle θ_S^*. The position of the conversion point on the reflector depends on the apparent dip angle φ_{AD} and, through θ_S^*, also on the ratio r. For φ_{AD} approaching 0°, $\bar{x}_{Clim}$ in the second equation of (A-12) approaches 1 as it was the case for $\varphi_{AD} < 0^\circ$, see Eq. (A-11). For φ_{AD} increasing, $\bar{x}_{Clim}$ decreases and becomes zero for $\tan\theta_S^* \tan\varphi_{AD} = 1$. For $\tan\theta_S^* \tan\varphi_{AD} > 1$, the first equation of (A-12) must be used. The solution $\bar{x}_{Clim} = 0$ corresponds to the conversion point coinciding with the source S and the S-wave ray leg parallel to the source-receiver profile.

Inserting the above expressions for $\bar{x}_{Clim}$ to Eq. (A-10), we obtain the coefficient C_3 for any combination of the apparent dip angle φ_{AD} and the ratio r.

For $r = 1$, Eq. (A-10) yields $C_3 = 0$ because $C_0 = 1/2$, $C_1 = -\sin\varphi_{AD}/4$, $C_2 = 0$ and $\bar{x}_{Clim} = 0$ for $\varphi_{AD} > 0^\circ$ and $\bar{x}_{Clim} = 1$ for $\varphi_{AD} < 0^\circ$. Inserted to Eq. (A-7), this yields

$$x_C \sim \frac{x}{2}\frac{H_S}{H} . \qquad (A-13)$$

Comparing Eq. (A-13) with (A-6), we can conclude that for $r = 1$, approximate Eq. (A-7) yields the exact solution of Eq. (A-4).

From Eq. (A-4), we can see that the offset x_C of the conversion point depends on the offset x, the distance H, apparent dip angle φ_{AD} and through the ratio r of the S- and P-wave velocities on the parameters of the reference medium.

In Fig. 6, on the graphs of the variation of the ratio x_C/x with the normalized offset x/H we compare values of x_C obtained from approximate formula (A-7) (dashed curve) with values x_C obtained by numerical solution of the quartic equation (A-4) (solid curve). The curves correspond to the P-S-wave conversion in the isotropic layer with P- and S-wave velocities $\alpha = 2.5$ km/s and $\beta = 1.$ km/s, i.e., with the ratio of S- and P-wave velocities $r = 0.4$. The following apparent dip angles φ_{AD} are considered: $\varphi_{AD} = 0^\circ$ - black, $\varphi_{AD} = 10^\circ$ - red, $\varphi_{AD} = 20^\circ$ - blue, $\varphi_{AD} = -10^\circ$ - green, $\varphi_{AD} = -20^\circ$ - light blue. Because x_C is the solution of Eq. (A-4), which depends on the ratio r, the value of the ratio x_C/x for $x = 0$ depends on r too. We can see that the formula (A-7) yields satisfactory results. For $x_{max} < 8$, it converges correctly to x_{Clim}.

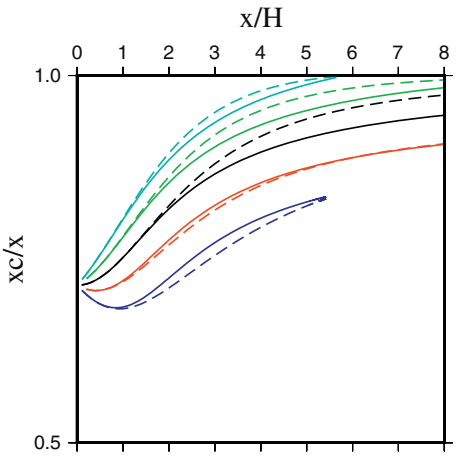

Fig. 6. Variation with the normalized offset x/H of the ratio x_C/x for the P-S-wave in the isotropic layer with the ratio of S- and P-wave velocities $r = 0.4$. Varying apparent dip angle φ_{AD} considered: $\varphi_{AD} = 0^\circ$ - black, $\varphi_{AD} = 10^\circ$ - red, $\varphi_{AD} = 20^\circ$ - blue, $\varphi_{AD} = -10^\circ$ - green, $\varphi_{AD} = -20^\circ$ - light blue. Full curves correspond to x_C obtained by numerical solution of quartic equation (A-4), dashed curves to approximate solution (A-7) with C_i defined in Eqs. (A-8) and (A-10).

Appendix B. WA parameters used in the study

In the Cartesian coordinate system related to the reflector, WA parameters ϵ_x, ϵ_z, δ_y and γ_y used in Eqs. (7), (8), (10) and (11) of the main text are defined as

$$\epsilon_x = \frac{A_{11} - \alpha^2}{2\alpha^2}, \quad \epsilon_z = \frac{A_{33} - \alpha^2}{2\alpha^2}, \quad \delta_y = \frac{A_{13} + 2A_{55} - \alpha^2}{\alpha^2}, \quad \gamma_y = \frac{A_{55} - \beta^2}{2\beta^2} . \qquad (B-1)$$

Here A_{11}, A_{13}, A_{33} and A_{55} denote density-normalized elastic moduli in the Voigt notation, specified in the above-mentioned Cartesian coordinate system, and α and β are P- and S-wave velocities in the reference isotropic medium. By choosing $\alpha^2 = A_{33}$ and $\beta^2 = A_{55}$, we have $\epsilon_z = \gamma_y = 0$. The WA parameter ϵ_x becomes equivalent to ϵ of Thomsen (1986), but WA parameter δ_y is different from δ of Thomsen (1986).

References

Alkhalifah, T., Sava, P., 2010. A transversely isotropic medium with a tilted symmetry axis normal to the reflector. Geophysics 75, A19–A24.

Farra, V., Pšenčík, I., 2010. Coupled S waves in inhomogeneous weakly anisotropic media using first-order ray tracing. Geophys. J. Int. 180, 405–417.

Farra, V., Pšenčík, I., 2013a. Moveout approximations for P and SV waves in VTI media. Geophysics 78, WC81–WC92.

Farra, V., Pšenčík, I., 2013b. Moveout approximations for P and SV waves in dip-constrained transversely isotropic media. Geophysics 78, C53–C59.

Farra, V., Pšenčík, I., 2017. Reflection moveout approximation for a converted PSV wave in a moderately anisotropic homogeneous VTI layer. Seismic Waves in Complex 3-D Structures. 27, pp. 51–58.

Farra, V., Pšenčík, I., Jílek, P., 2016. Weak-anisotropy moveout approximations for P waves in homogeneous layers of monoclinic or higher anisotropy symmetries. Geophysics 81, C39–C59.

Gajewski, D., Pšenčík, I., 1990. Vertical seismic profile synthetics by dynamic ray tracing in laterally varying layered anisotropic structures. J. Geophys. Res. 95, 11301–11315.

Golikov, P., Alkhalifah, T., Stovas, A., 2012. Prestack traveltimes for dip-constrained TI media. 82nd Annual International Meeting, SEG, Expanded Abstracts https://doi.org/10.1190/segam2012-0507.1.

Granli, J.R., Arntsen, B., Sollid, A., Hiide, E., 1999. Imaging through gas-filled sediments using marine shear-wave data. Geophysics 64, 668–677.

Hao, Q., Stovas, A., 2016. Generalized moveout approximation for P-SV converted waves in vertically inhomogeneous transversely isotropic media with a vertical symmetry axis. Geophys. Prospect. 64, 1469–1482.

Li, X.-Y., Yuan, J., 2003. Converted-wave moveout and conversion-point equations in layered VTI media: theory and applications. J. Appl. Geophys. 54, 297–318.

Seriff, A.J., Sriram, K.P., 1991. P-SV reflection moveouts for transversely isotropic media with a vertical symmetry axis. Geophysics 56, 1271–1274.

Tessmer, G., Behle, A., 1988. Common reflection point data-stacking technique for converted waves. Geophys. Prospect. 36, 671–688.

Thomsen, L., 1986. Weak elastic anisotropy. Geophysics 51, 1954–1966.

Thomsen, L., 1999. Converted-wave reflection seismology over inhomogeneous anisotropic media. Geophysics 64, 678–690.

Tsvankin, I., 2001. Seismic Signatures and Analysis of Reflection Data in Anisotropic Media. Elsevier Science Ltd, Oxford.

Tsvankin, I., Grechka, V., 2000. Dip moveout of converted waves and parameter estimation in transversely isotropic media. Geophys. Prospect. 48, 257–292.

Tsvankin, I., Grechka, V., 2011. Seismology of Azimuthally Anisotropic Media and Seismic Fracture Characterization. SEG.

Tsvankin, I., Thomsen, L., 1994. Nonhyperbolic reflection moveout in anisotropic media. Geophysics 59, 1290–1304.